Pergamon

PII: S0301-9322(97)00004-9

Int. J. Multiphase Flow Vol. 23, No. 4, pp. 713–723, 1997

Printed in Great Britain
0301-9322/97 $17.00 + 0.00

CHAOTIC BUBBLE COALESCENCE IN NON-NEWTONIAN FLUIDS

H. Z. LI[1], Y. MOULINE[1], L. CHOPLIN[1] and N. MIDOUX[2]

[1]Centre de Génie Chimique des Milieux Complexes, [2]Laboratoire des Sciences du Génie Chimique, CNRS-ENSIC-INPL, 1 rue Grandville, BP 451, 54001 Nancy Cedex, France

(Received 25 August 1996; in revised form 5 February 1997)

Abstract—This work aims at studying in-line bubble coalescence in non-Newtonian fluids. The visualisation and power spectrum of time series data, recorded via an optical sensing device, confirm that the bubble formation at the orifice is perfectly periodic under a constant gas flowrate. However, the separation interval between bubbles becomes irregular during rise, until, at a certain height above the orifice, the coalescence occurs. An original approach is elaborated by relating the rise of a chain of bubbles to consecutive shear deformations. A series of measurements on a rheometer proves for the first time that the bubble coalescence is mainly governed by the dynamical competition between the creation and relaxation of shear stresses. The time delay embedding method of reconstructing the phase-space diagram is applied to time series data recorded at different heights in the bubble column. The calculation of several parameters: the largest Lyapunov exponent, the correlation dimension, the power spectrum, and the phase portraits, reveals that the coalescence between bubbles obeys a chaotic and deterministic mechanism. © 1997 Elsevier Science Ltd.

Key Words: chaos, bubble, coalescence, interactions, non-Newtonian fluid

1. INTRODUCTION

The behaviour of bubbles, especially their coalescence, in non-Newtonian fluids is of key importance in such diverse fields as polymer devolatilisation, composites processing, boiling, bubble column, fermentation, cavitation, plastic foam processing, bubble absorption, etc. However, basic knowledge is still missing concerning the coalescence of bubbles in both Newtonian and non-Newtonian fluids.

Compared with the understanding of bubbles in Newtonian fluids, the study of the bubble behaviour in non-Newtonian fluids remains still in an elementary stage. Due to the inherent complex nature of bubble phenomena, a complete theoretical analysis is impossible at present. A somewhat simplified starting point in this field has been the study of bubbles formed from a single submerged orifice, which excludes mutual influence of bubbles formed in neighbouring orifices. Until now, little attention was paid to studies of bubble coalescence (Trambouze 1993). Nevertheless, the loss of interfacial area due to coalescence can be a serious matter in industrial gas–fluid installations.

The final stage of coalescence is the rupture of the thin film of non-Newtonian fluid separating two bubbles, a matter that has received some attention (Acharya and Ulbrecht 1978; De Kee *et al.* 1990). However, an equally important problem, about which there is no information in the literature, is the governing mechanism by which bubbles draw together and coalesce. This is the topic for consideration in the present paper.

2. BASIC CONCEPTS: SOME DEFINITIONS

Chaos theory is a newly developing discipline, we recommend the books by Bergé *et al.* (1984), Schuster (1988) and Ott (1993) as good overviews. To facilitate the understanding, the basic definitions are given below without resorting to too much mathematics before presenting results.

In mathematical models of physical dynamical systems, the dynamic evolution is visualised in the phase-space whose dimension is given by the number of independent variables. In experiments, the phase-space is usually unknown beforehand and often only a single scalar variable of the system (a single time series) can be measured. Fortunately, it can be shown that one variable already contains most of the information about the total system and not just a minor part (Takens 1981; Mañé 1981). A widely used method of reconstructing a phase-space from a single time series has been proposed by Packard *et al.* (1980). The dynamics of a time series $\{x_1, x_2, \ldots, x_n\}$ are fully embedded in the D-dimensional phase-space $\mathbb{R}^D (D > d$, where d is the dimension of the attractor) defined by

$$Y_t = \{x_t, x_{t+\tau}, x_{t+2\tau}, \ldots, x_{t+(D-1)\tau}\}, \quad [1]$$

where τ is a suitably selected delay time. If the time series is sampled every Δt s, then the delay parameter may be expressed as $\tau = J\Delta t$.

2.1. Correlation dimension ν

The correlation dimension ν has been used as a characteristic of strange attractors to distinguish between deterministic chaos and stochastic processes (Grassberger and Procaccia 1983). The fundamental difference results in the existence of an underlying order for deterministic chaos (Rodriguez-Iturbe *et al.* 1989). In a way, the correlation dimension measures the efficiency of the variables in taking up space in various dimensions. The correlation dimension ν is defined as

$$\nu = \lim_{r \to 0} \frac{\log C(r)}{\log r}, \quad [2]$$

where r is the radius of an D-dimensional sphere and $C(r)$ is the so-called correlation integral:

$$C(r) = \lim_{N \to \infty} \frac{1}{N^2} \sum_{i,j=1}^{N} H(r - \| Y_i - Y_j \|), \quad i \neq j \quad [3]$$

where H is the Heaviside step function, N the number of points in (Y_t), and $\| Y_i - Y_j \|$ a suitable norm, e.g. the Euclidean norm which is used in this study.

For stochastic processes, ν varies linearly with increasing the phase-space dimension D without reaching a saturation value, whereas for deterministic chaos, the value of ν levels off after a certain D (Bergé *et al.* 1984).

2.2. Lyapunov exponents λ_i

Chaotic systems exhibit sensitive dependence on initial conditions. This expression has been introduced to denote the property of a chaotic system, that small differences in the initial conditions, however small, are persistently magnified because of the dynamics of the system, so that in a finite time the system attains totally different states. The notion of sensitive dependence on initial conditions is made more accurate through the introduction of Lyapunov exponents. Usually, systems containing at least one positive Lyapunov exponent are considered to be chaotic (Wolf *et al.* 1985; Benettin *et al.* 1980). This means that trajectories starting from two nearby points, no matter how close together, will evolve quite differently and move exponentially away from one another with time.

The implementation of the algorithm of Wolf *et al.* (1985) is straightforward. The distance between the initial point $x(t_0)$ and the nearest neighbour is denoted $L(t_0)$. At time t_1, this length element will evolve to $L'(t_1)$. When $L'(t_1)$ becomes too large, a new $L(t_1)$ is defined. In addition to a small $L(t_1)$, the angular separation between the evolved and replacement elements must also be small. This procedure is repeated throughout the entire phase-space. With M being the total number of replacement steps, the largest Lyapunov exponent λ_1 is estimated from the following expression:

$$\lambda_1 = \frac{1}{N\Delta t} \sum_{i=1}^{M} \log_2 \frac{L'(t_i)}{L(t_{i-1})}. \quad [4]$$

When $\lambda_1 > 0$, it means that the time series has at least one positive Lyapunov exponent and the series is then chaotic. When $\lambda_1 \leqslant 0$, the time series is a regular motion process.

2.3. Power spectrum

Chaotic motion means that the signal $x(t)$ displays an irregular and aperiodic behaviour in time. One of the qualitative methods used to distinguish between chaotic or periodic behaviour is a power spectral analysis which consists of Fourier transforming the signal $x(t)$:

$$X(f) = F[x(t)] = \int_{-\infty}^{+\infty} x(t)e^{-j2\pi ft}dt. \quad [5]$$

The power spectrum of the signal can then be calculated by

$$P(f) = |X(f)|^2. \quad [6]$$

The power spectrum of a periodic behaviour consists of only discrete lines of the corresponding frequencies, whereas chaotic behaviour is completely aperiodic, and exhibits then broadened spectral lines with no dominant frequencies in $P(f)$ that are mostly located at low frequencies (Schuster 1988).

3. EXPERIMENTAL

Figure 1 shows the main features of the experimental set-up consisting of a Plexiglas cylindrical tank surrounded by a square duct. The diameter of the tank was 0.30 m and its height was 0.40 m. The duct had a 0.35 m square cross section, and permitted to eliminate optical distortions for visualization as well as to control the liquid temperature inside the cylindrical tank. Bubble generation was through an orifice of varying diameters ($0.2–5 \times 10^{-3}$ m), submerged in the liquid at the centre at the bottom section of the tank. Air was used as injected gas. A great reservoir was used to avoid any fluctuations due to bubble formation and detachment. The air injection system was designed in order to be operated in two different ways. When a continuous flowrate was applied, the electronic valve of rapid response ($\leqslant 8$ ms) controlled by a personal computer was kept

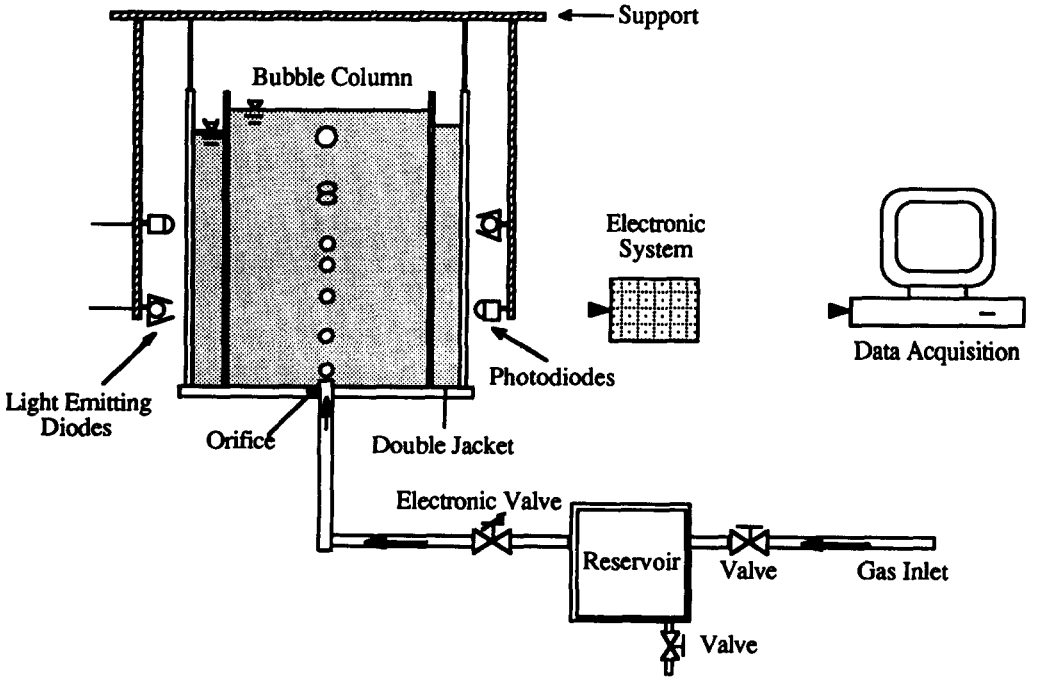

Figure 1. Experimental set-up.

open so that the air entered into the fluid and formed a set of bubbles rising in line. By means of camera visualization and image analysis, it was observed that under a stationary flowrate, the bubbles formed in line had the same shape and identical volume. However, the injection period between bubbles was fixed with a continuous injection. It was possible to inject a set of bubbles of determined volume with a desired injection period through the electronic valve by varying its open duration as well as the pressure inside the reservoir.

In this study, the time series data were the frequency of bubble passage at different heights in the tank. They were measured by optical probes of photodiodes placed at the external wall of the square duct. The data acquisition was carried out by the personal computer. All experiments were carried out at constant temperature (293 K).

The non-Newtonian fluids used in this work were 1% (wt) polyacrylamide (PAAm) in 99% water, 1.5% (wt) PAAm in 49.25% (wt) water—49.25% (wt) glycerol and 1.7% (wt) carboxymethylcellulose (CMC) in 44.6% (wt) water—53.7% (wt) glycerol. A Rheometrics Fluid Spectrometer RFS II was employed to measure the rheological properties of these solutions which behaved as shear-thinning fluids (figure 2). They can be perfectly fitted by the Cross model. As normal stresses were too small to be measured accurately in these fluids, stress relaxation measurements after sudden cessation of steady shear flow were performed. At the same shear rate, the relaxation times for the CMC, 1% PAAm and 1.5% PAAm solutions were respectively of the order of 2, 9 and 15 s. Therefore, the 1.5% PAAm solution may be seen as the most elastic, while the CMC solution is the least one.

4. RESULTS AND DISCUSSION

Typically, in-line interactions will accelerate the bubble rise velocity in Newtonian fluids (Omran and Foster 1977). The evidence of this behaviour in non-Newtonian fluids was clearly brought up in this work: the influence of the injection period on the rise velocity is shown in figure 3 in the 1% PAAm solution. An injection period of order of 3, 10 and 15 s was necessary to prevent the

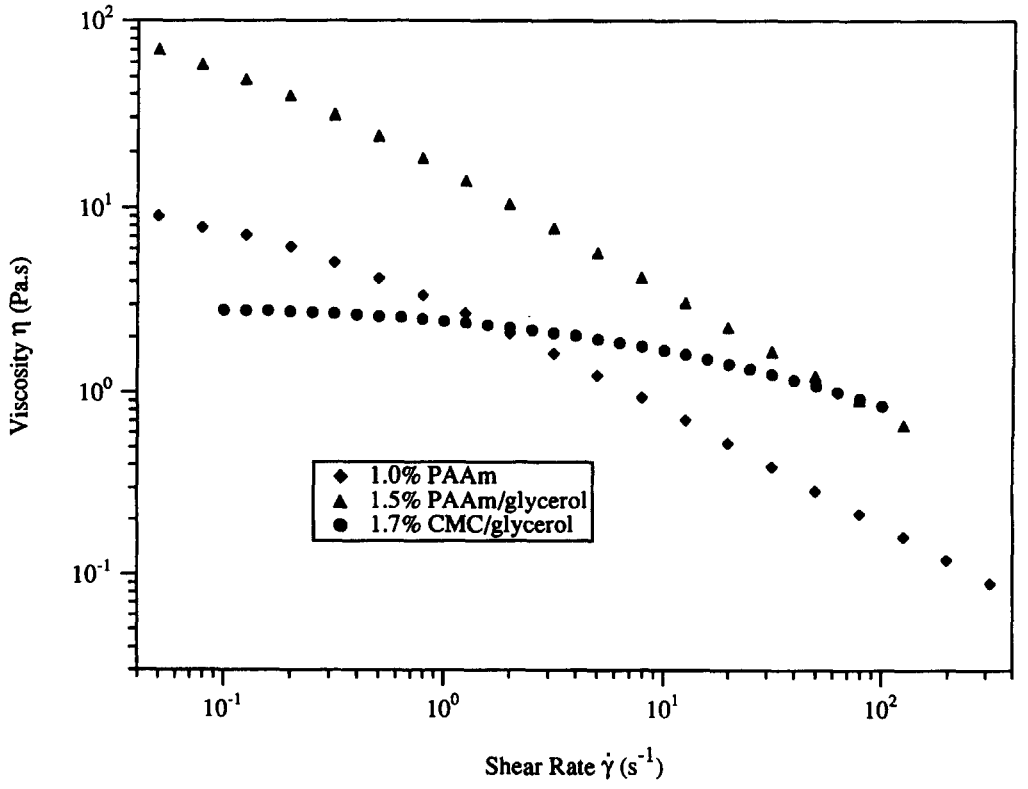

Figure 2. Variation of the viscosity vs the shear rate.

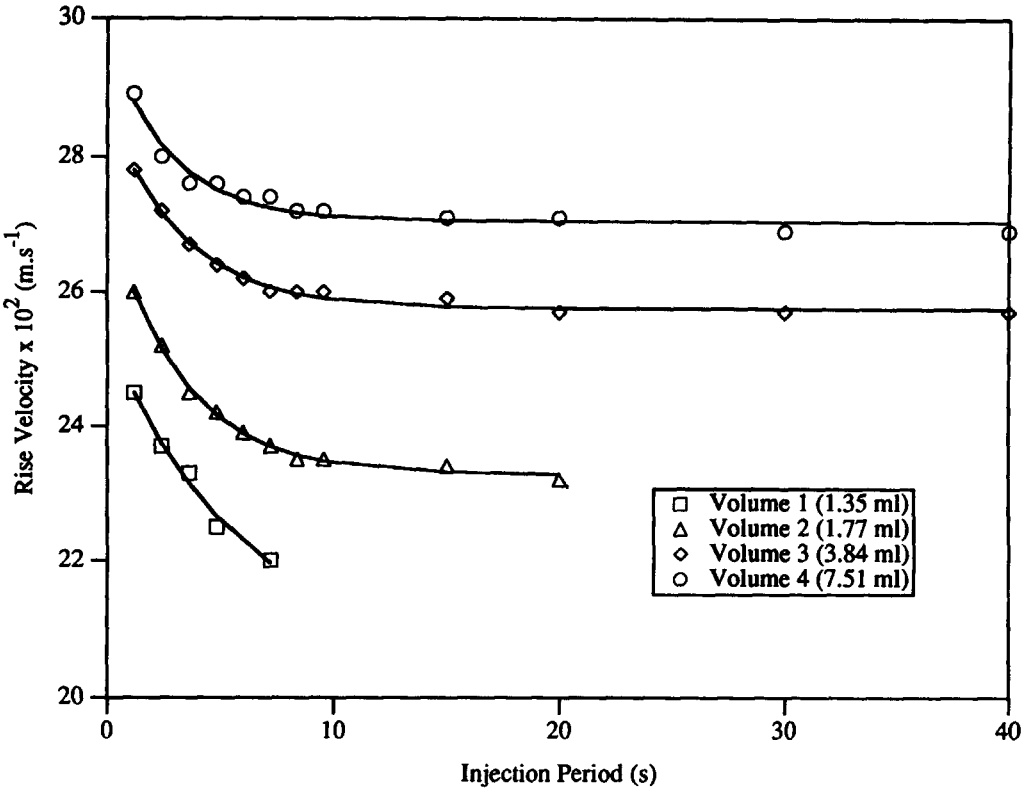

Figure 3. Influence of the injection period on the rise velocity in 1% PAAm solution.

interactions between bubbles, respectively for the CMC, 1% PAAm and 1.5% PAAm fluids. Approximately, this is nothing but the rough estimate of the stress relaxation time obtained on the rheometer. In the absence of interactions, the bubble rise velocity increased with the volume and the dependence upon the orifice diameter seemed to be negligible. The latter can be explained by the fact that compared with the bubble formation in water, the viscous resistance due to the high value of fluid viscosity in this study (800–6000 times more viscous than water) should be dominant with respect to the inertial effects. When the injection period became short enough (less than 1 s), an interesting phenomenon was observed: from a certain rising distance from the orifice according to the operating parameters (in general about 10 cm), a trailing bubble began to accelerate progressively, and approached the leading bubble who kept nevertheless its rising velocity. When the trailing bubble was very close to the leading one, these two bubbles underwent progressively shape changes, especially at the level of the tail for the leading bubble and the top for the trailing one to form two parallel interfaces. They collided and coalescence occurred. The bubble chain was then broken up. The coalesced bubble accelerated the rise velocity due to the increase of the volume and induced consecutive coalescence. In this case, the measurement of a stationary rise velocity is meaningless.

In the literature, the interactions and coalescence of bubbles are a little better documented for Newtonian fluids, especially for water. In this case, the acceleration of the trailing bubble is usually considered as based on a decreased drag within small distance, due to turbulence in the viscous wake induced by the leading one (De Nevers and Wu 1971; Bhaga and Weber 1980).

Respectively, by means of a visualization method and a laser–Doppler anemometer, Coutanceau and Hajjam (1982) and Bisgaard (1983) have observed a peculiar phenomenon behind the leading bubble in a non-Newtonian fluid: the fluid went up with the bubble only in its vicinity; from a close distance behind the bubble, the fluid took an opposite direction and went down to form a 'negative wake'. The exact length of the negative wake is difficult to determine, because the negative velocity approaches zero very slowly. This effect is in general attributed to the elasticity of the fluid, but requires further theoretical and experimental investigation.

Effectively, the wake behind a leading bubble can be considered responsible for the decreased drag in water. On the other hand, the negative wake in a non-Newtonian fluid is not likely to explain the interactions and coalescence in non-Newtonian fluids. With respect to water, the high value of the viscosity of the non-Newtonian fluids used in this work will also easily absorb any turbulence created by the passage of a bubble. It may be noticed that compared with bubble rise in water, the Reynolds number is 800–6000 times smaller in our fluids. Furthermore, an another significant factor differentiating bubble–bubble interactions in non-Newtonian fluids from that in water is the long field of action. In the PAAm solutions, a following bubble can accelerate from a distance of 0.4 m behind the leading one which is reaching the free surface. In a higher column, the interaction range could be expected to cover greater distance. Consecutive coalescence will produce bigger bubbles and affect then seriously the transfer efficiency as this is the case in an industrial fermentor.

A more plausible explanation may be the relaxation of stresses induced by the passage of bubbles. The relaxation time of these stresses is determined by the fluid elasticity. However, a rigorous modelling of the interactions between bubbles is beyond the reach until now. So, we had the idea to simulate the passage of bubbles by imposing consecutive shear rates to a fluid sample by means of the rheometer RFS II which measured the response of the sample in term of stress. We call this original approach 'rheological simulation' (Li *et al.* 1997). In the literature, the maximum shear rate corresponding to the rise of a bubble is defined as the ratio of the rise velocity to the equivalent diameter of the bubble: $\dot{\gamma}_{max} = v/d_{eq}$. For the passage of a chain of bubbles formed under a constant injection period T at a point in fluid for consideration, the simulated shear rate of each bubble was calculated by a periodic function of hyperbolic cosine kind.

The rheological simulation showed that there was a gradual accumulation of stresses which had tendency to reach a stationary value. The magnitude of these unrelaxed or residual stresses could be considered as both strongly dependent upon the injection period and proportional to the elasticity of the fluid. In the light of these findings, the following scenario can be proposed: after the passage of a leading bubble, the memory effect of the elasticity holds the shear-thinning process during a certain time so that the local viscosity decreases, and the drag opposed to the trailing bubble is then reduced.

The rheological simulation was realised in these three fluids, taking especially into account the experimental values of rise velocity and injection period. Figure 4 reports a qualitative comparison between the reduced rise velocity and the reduced residual stress (normed respectively by the stationary rise velocity and initial stress) as a function of the injection period. In spite of the scale difference between these two parameters, a close correlation does exist and provides evidence that the interactions should be essentially dominated by stress relaxation process. It is worth noting that to our knowledge, such an approach is not yet reported in the literature.

Analysis of chaotic time series involves calculating dynamical invariants or dimensions. These parameters are the best available measure to describe and quantify the underlying attractor of a chaotic system. Specifically, the present study employs four techniques for chaotic behaviour analysis. The power spectrum, phase portrait, Lyapunov exponent, and correlation dimension analyses were used to determine the presence of strange attractor and chaotic behaviour in bubble coalescence caused by non-linear interactions between bubbles.

The tendency of these solutions were comparable. In this paper, only the results of 1% PAAm solution with an air flowrate of $0.18 \times 10^{-6}\ m^3\ s^{-1}$ are presented. Figure 5 shows an example of the temporal measurements at, respectively, 1.5 and 15 cm above the orifice. Each pulse corresponds to the passage of a bubble. When a bubble passed in front of the optical probes, a part of light was reflected so that the signal in form of electric voltage detected by the photodiodes decreased and could become negative. It is very interesting to note that at a height near the orifice, the bubble passage was very regular with similar pulses and constant intervals between them. Due to the coalescence, this regularity was progressively lost with the increase of the height. At 15 cm above the orifice, the number of bubbles decreased drastically and the magnitude of some pulses increased significantly due to the increase of bubble size. Figure 6 shows the corresponding power spectrum of bubble passage at, respectively, 1.5 and 15 cm above the orifice. Near the orifice, the principal frequency followed by a set of harmonics demonstrates that the formation of bubble was perfectly periodic. This was confirmed by visual observation and image analysis. However, this

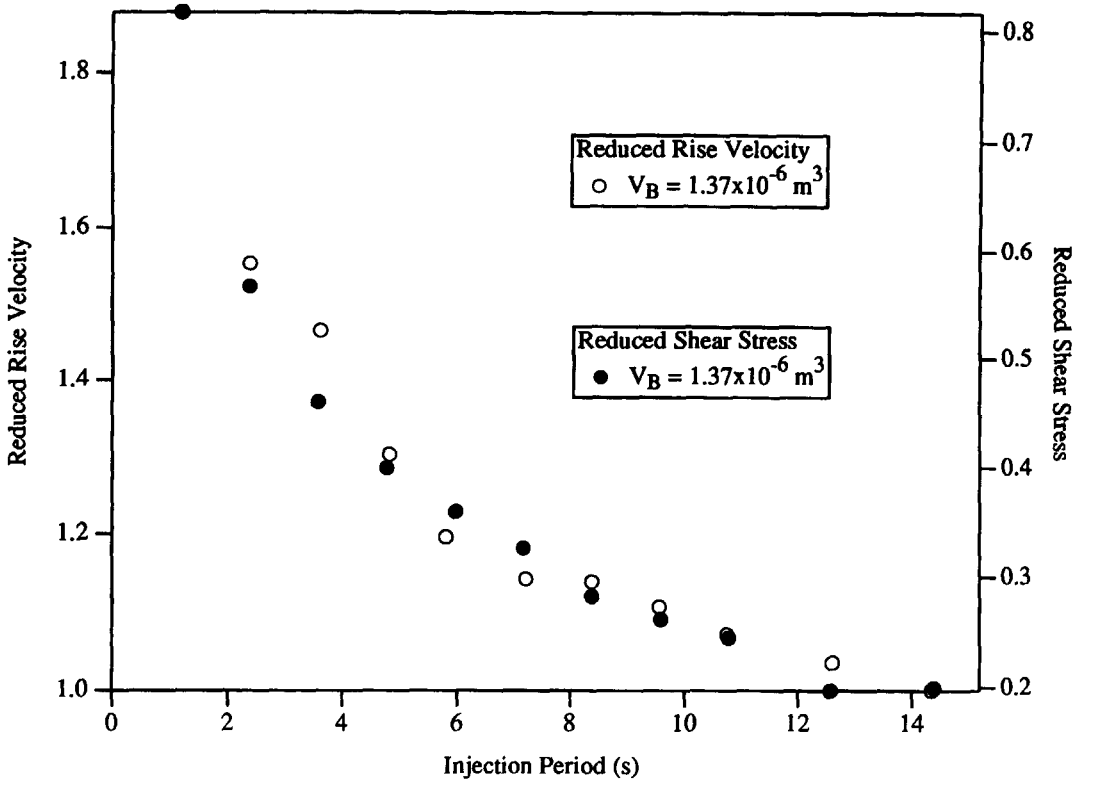

Figure 4. Agreement between the reduced rise velocity and reduced residual stresses in function of the injection period in 1.5% PAAm solution (bubble volume: 1.37×10^{-6} m^3).

regularity was progressively lost when the distance from the orifice increased, and the power spectrum is typically that of a chaotic phenomenon, since it exhibits broadened spectral lines with no dominant frequencies in the power spectrum that are mostly located at low frequencies.

As shown above, it is possible to reconstruct new coordinates by means of the time delay embedding technique: $X = x_t$ and $Y = x_{t+\tau}$ (the delay parameter $\tau = \Delta t$) in order to represent the corresponding phase portrait (figure 7). It is worth noting that at 1.5 cm, the phase portrait shows a regular ring symbolising a mono-frequencial phenomenon. On the other hand, the phase portrait at 15 cm reveals a very rich structure of the attractor with the appearance of several rings that

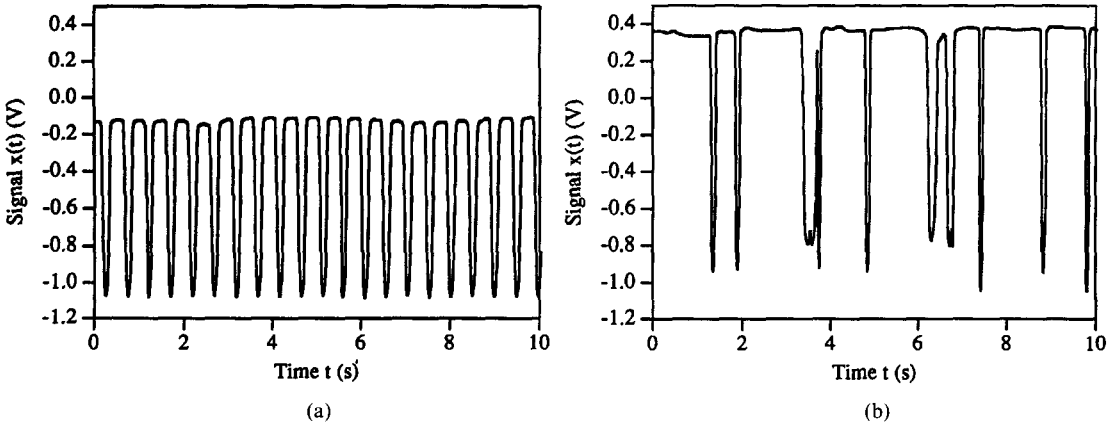

Figure 5. Temporal measurements of the bubble passage at (a) 1.5 cm and (b) 15 cm from the orifice in 1% PAAm solution ($Q = 0.18 \times 10^{-6}$ m^3 s^{-1}).

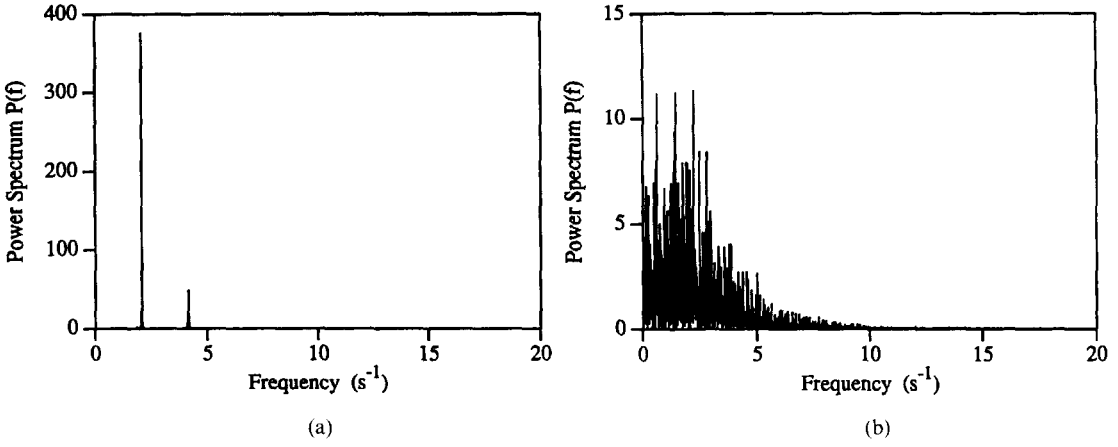

Figure 6. Power spectrum of the signals (figure 5) at (a) 1.5 cm and (b) 15 cm above the orifice.

characterize consecutive coalescence of bubbles: the formation of each ring in the phase portrait introduces a new independent frequency. In relation to the phase portraits, a close examination of the frequency appearance in the power spectrum especially in function of different heights above the orifice tends to show that the period-doubling sequences could be the most plausible route to lead to chaos. However, the rigorous determination of the route requires still further investigation.

According to the phase portraits, it is then possible to speculate that in order to describe consecutive coalescence and to predict the final bubble size in a very high industrial bubble column, the self-similar structure could lead to a scaling law through a fractal dimension from laboratory pilot to industrial installation.

The computation of the largest Lyapunov exponent λ_1 is subject to the utmost care. In fact, the absolute value of λ_1 is very sensitive to the parameters required in the algorithm of Wolf *et al.* (1985): embedding dimension D, minimum and maximum length scales, number of replacement steps M, the number of data points N and especially the delay time τ. The values of the largest Lyapunov exponent λ_1 at different heights in the column are presented in table 1. In the middle column of this table, the delay time τ is simply the data acquisition interval as commonly used in the literature. In the right column, the delay time τ was optimized for each time series by using the method proposed by Rosenstein *et al.* (1994). Clearly, the results are quite different according to the delay time and the number of data points used. In spite of the difference in absolute magnitude, there is a certain convergent tendency. The exponent is negative or close to zero for the regular bubble passage near the orifice. An abrupt increase of λ_1 is observed when the coalescence took place. The exponent decreases as bubbles approached the top of the column. This decrease might be explained as follows: the bubble passage became more regular due to the drastic

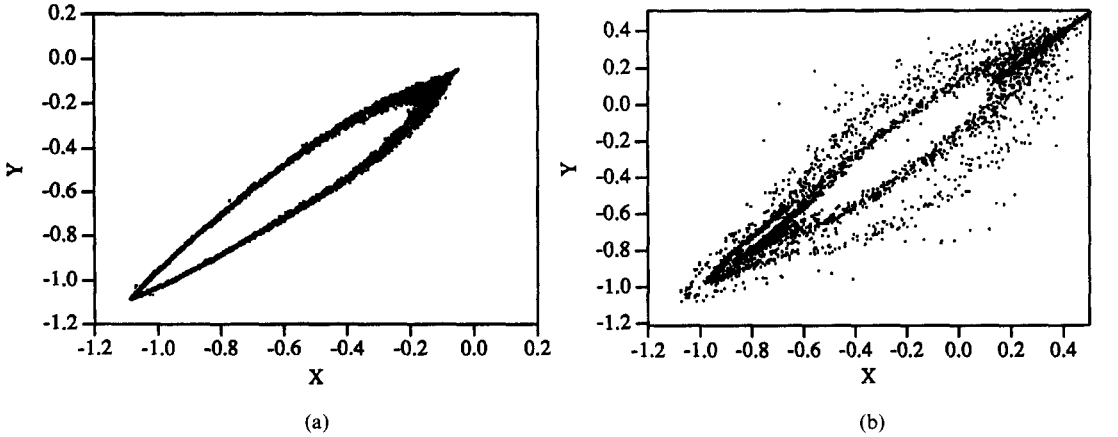

Figure 7. Phase portraits of the signals (figure 5) at (a) 1.5 cm and (b) 15 cm above the orifice.

Table 1. The largest Lyapunov exponent λ_1 at different heights in the column

Distance from the orifice (cm)	Largest Lyapunov exponent λ_1 ($N = 8192$ points and $\tau = \Delta t$)	Largest Lyapunov exponent λ_1 ($N = 16384$ points and τ optimized)
1.5	−0.17	0.001 ($\tau = 5\Delta t$)
4.8	−2.80	0.002 ($\tau = 5\Delta t$)
7.0	0.58	0.2 ($\tau = 5\Delta t$)
9.5	14.90	1.8 ($\tau = 5\Delta t$)
12.1	16.99	1.9 ($\tau = 5\Delta t$)
15.0	37.25	1.9 ($\tau = 4\Delta t$)
19.8	15.10	1.8 ($\tau = 4\Delta t$)
27.3	−18.09	1.0 ($\tau = 4\Delta t$)
33	−7.6	0.9 ($\tau = 4\Delta t$)

decrease of bubble number resulting from the consecutive coalescence in the lower column section (for the same measurements duration, the bubble number decreased from 2000 bubbles near the orifice to about 500 bubbles at the approach of the top of the column); moreover, the free surface could slow down the bubble rise and introduce to a certain extent some orders.

The variation of the correlation dimension with the embedding dimension is shown in figure 8 for the measurements at 15 cm in the column. It can be seen that the saturation value is achieved when $D = 3$. This gives estimates of the lower bounds for the dimension of embedding phase space sufficient to model the dynamics. In another words, the number of degrees of freedom in the chaotic coalescence is only 3. This means that three ordinary differential equations would be sufficient to describe the chaotic coalescence procedure.

The search of the form of such equations is being carried out. We will try to make use of the rheological properties of the fluids, in particular the relaxation function. The knowledge of these equations will also help to understand the route leading to chaos in the coalescence of bubbles. Furthermore, compared with Kaplan–Yorke conjecture, the value of the correlation dimension

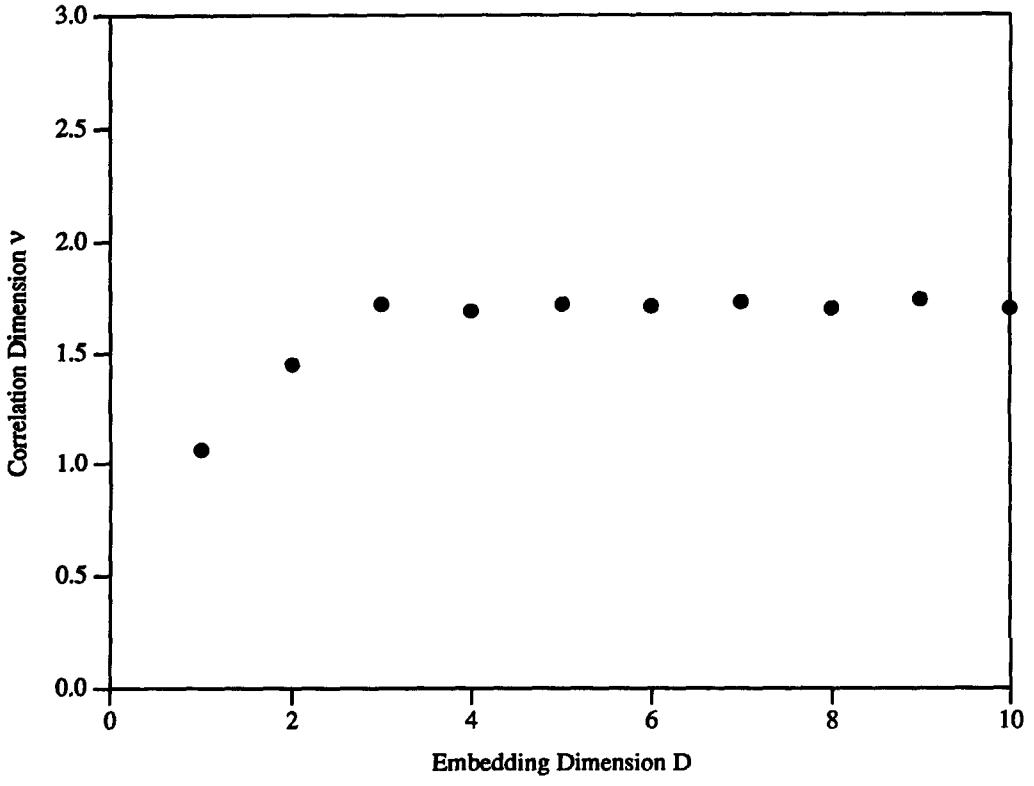

Figure 8. Variation of the correlation dimension with the embedding dimension at 15 cm above the orifice.

obtained shows that the method proposed by Rosenstein *et al.* (1994) to calculate the delay time τ is relatively suitable for computing the largest Lyapunov exponent λ_1.

5. CONCLUSIONS

This work reports a study of in-line bubble coalescence in non-Newtonian fluids. The image analysis show that under a constant gas flowrate, bubbles formed at the orifice have the identical volume, shape and separation interval. As bubbles rise in the column, the separation interval between bubbles becomes irregular, until, at a height with respect to the orifice, the coalescence occurs.

The original rheological simulation, taking into account the experimental injection period and bubble rise velocity, throws insight for the first time to the accumulation of residual stresses in non-Newtonian fluids after the passage of a chain of bubbles. The relaxation of these residual stresses, closely related to the drag decrease, is then the dominant mechanism governing the interactions and coalescence between bubbles. The time delay embedding method of reconstructing the phase-space diagram was applied to time series data of bubble passage recorded at different heights in the bubble column. The power spectrum shows that near the orifice, the principal frequency is followed by a set of harmonics: the formation of bubbles is then perfectly periodic. However, this periodicity is progressively lost with the increasing distance from the orifice, and the power spectrum exhibits broadened spectral lines with no dominant frequencies. The appearance of chaos can also be visualised through phase portraits: the formation of several rings reveals the frequency bifurcation. The largest Lyapunov exponent is negative or close to zero for the regular bubble passage near the orifice. An abrupt change occurs when the coalescence takes place. The variation of the correlation dimension with the embedding dimension reaches a saturation value when the embedding dimension is equal to 3. This gives estimates of the lower bounds for the dimension of embedding phase-space sufficient to model the dynamics. It is then possible to attribute the appearance of the chaos to a non-linear dynamical competition between the creation and relaxation of shear stresses as shown by the rheological simulation. The third control parameter would be the bubble formation frequency at the orifice.

In the light of these results, the establishment of future models for bubble coalescence will be hoped possible in non-Newtonian fluids.

Acknowledgements—The authors would like to thank Professor Gianni Astarita for the very helpful discussions. The financial assistance provided by the Consortium of Industrial Companies: Elf-Atochem, Lafarge, Michelin, Rhône-Poulenc Industrialisation and Total (Cray Valley) is gratefully acknowledged.

REFERENCES

Acharya, A. and Ulbrecht, J. (1978) Note on the influence of viscoelasticity on the coalescence rate of bubbles and drops. *AIChE J.* **24,** 348–351.

Astarita, G. and Apuzzo, G. (1965) Motion of gas bubbles in non-Newtonian liquid. *AIChE J.* **11,** 815–820.

Benettin, G. L., Galgani, A. G. and Strelcyn, J. M. (1980) Lyapunov characteristic exponents for smooth dynamical systems and for Hamiltonian systems: a method for computing all of them. Part 1: theory. *Meccanica* **15,** 9–20.

Bergé, P., Pomeau, Y. and Vidal, Ch. (1984) *L'ordre dans le chaos*. Hermann, Paris.

Bhaga, D. and Weber, W. E. (1980) In-line interaction of a pair of bubbles in a viscous liquid. *Chem. Eng. Sci.* **35,** 2467–2474.

Bisgaard, C. (1983) Velocity fields around spheres and bubbles investigated by laser–Doppler anemometry. *J. Non-Newtonian Fluid Mech.* **12,** 283–302.

Coutanceau, M. and Hajjam, M. (1982) Viscoelastic effect on the behaviour of an air bubble rising axially in a tube. *Appl. Sci. Res.* **38,** 199–207.

De Kee, D., Chhabra, R. P. and Dajan, A. (1990) Motion and coalescence of gas bubbles in non-Newtonian polymer solutions. *J. Non-Newtonian Fluid Mech.* **37,** 1–18.

De Nevers, N. and Wu, J. L. (1971) Bubble coalescence in viscous fluids. *AIChE J.* **17,** 182–186.

Grassberger, P. and Procaccia I. (1983) Measuring the strangeness of strange attractors. *Physica D* **9,** 189–208.

Li, H. Z., Mouline, Y., Choplin, L. and Midoux, N. (1997) Rheological simulation of in-line bubble interactions. *AIChE J.* **43,** 265–267.

Mañé, R. (1981) On the dimension of the conpact invariant sets of certain non-linear maps. In *Dynamical Systems and Turbulence*, ed. D. A. Rand and L. S. Young. Springer, Berlin.

Omran, N. M. and Foster, P. J. (1977) The terminal velocity of a chain of drops or bubbles in a liquid. *Trans. Inst. Chem.* **55,** 171–177.

Ott, E. (1993) *Chaos in Dynamical Systems*. Cambridge University Press, Cambridge.

Packard, N. H., Crutchfield, J. P., Farmer, J. D. and Shaw, R. S. (1980) Geometry from a time series. *Phys. Rev. Lett.* **45,** 712–716.

Rodriguez-Iturbe, I., De Power, B. F., Shariff, M. B. and Georgakakos, K. P. (1989) Chaos in rainfall. *Water Resour. Res.* **25,** 1167–1175.

Rosenstein, M. T., Collins, J. J. and De Luca, C. J. (1994) Reconstruction expansion as a geometry-based framework for choosing proper delay times. *Physica D* **73,** 82–98.

Schuster, H. G. (1988) *Deterministic Chaos*. VCH, Weinheim.

Takens, F. (1981) Detecting strange attractors in turbulence. In *Dynamical Systems and Turbulence*, ed. D. A. Rand and L. S. Young. Springer, Berlin.

Trambouze, P. (1993) Computational fluid dynamics applied to chemical reaction engineering. *Revue de l'Inst. Fr. Pétrole* **48,** 595–613.

Wolf, A., Swift. J. B., Swinney, H. L. and Vastano, J. A. (1985) Determining Lyapunov exponents from a time series. *Physica D* **16,** 285–317.